Gyrokinetic simulation of the FT-2 tokamak edge

L. Chôné[1], A. D. Gurchenko[2], E. Z. Gusakov[2], T. P. Kiviniemi[1],
S. I. Lashkul[2], S. Leerink[1], P. Niskala[1]

[1] *Department of Applied Physics, Aalto University, Espoo, Finland*

[2] *Ioffe Institute, St. Petersburg, Russia*

Predicting the dynamics of edge plasma is of particular importance for magnetic fusion devices. Indeed, the scrape-off layer (SOL) dynamics governs the power exhaust and plasma-surface interaction, which entails that it controls the influx of impurities, as well as the transition to improved confinement regimes via the formation of edge transport barriers (ETB) [1–5]. Because of the non-linear nature of the edge and SOL plasma dynamics, predictions have to rely on numerical simulations from first principle.

Here we perform full-torus simulations of electrostatic turbulence with the *ELMFIRE* gyrokinetic code [**?**,6,7]. The *ELMFIRE* code uses the particle-in-cell (PIC) method to solve the evolution of the full distribution functions of gyrokinetic ions and drift-kinetic electrons, and the gyrokinetic quasi-neutrality equation (QNE).

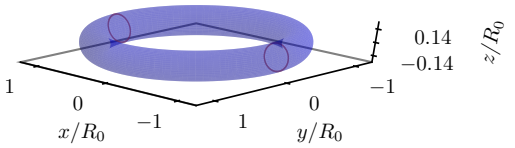

Figure 1: *Toroidal configuration for simulations of FT-2. The blue torus materialises the outer wall. The red circles are the poloidal limiter rings (punctual in the toroidal direction, in simulations).*

The magnetic background is an analytical toroidal equilibrium with circular concentric flux surfaces: $B = \frac{B_0}{1+\varepsilon\cos\vartheta}\left(\hat{e}_\varphi + \frac{\varepsilon}{q}\hat{e}_\vartheta\right)$, where $\varepsilon = r/R_0$ is the inverse aspect ratio, and q the safety factor. The gyrokinetic model used by *ELMFIRE* includes polarisation effects in the form of polarisation drift in the equations of motion (EMs) [9,10]. The EMs—for (R,U) the gyrocenter position parallel velocity—and QNE read:

$$\dot{R} = \frac{B^*U + E^*\times\hat{b}}{B^*_\parallel}, \quad \dot{U} = \frac{e_s}{m_s}\frac{B^*\cdot E^*}{B^*_\parallel} \tag{1}$$

$$\varepsilon_0\nabla\cdot E(r,t) = \sum_s e_s\int F_s\left\langle\delta\left(r-x^{(1)}\right)\right\rangle d^3RdUdJ \tag{2}$$

with:

$$E^* = \left\langle E\left(x^{(1)}\right)\right\rangle - \frac{J}{2\pi m_s}\nabla B - \frac{m_s}{e_s}\frac{d}{dt}\left[\frac{\left\langle E\left(x^{(1)}\right)\right\rangle\times\hat{b}}{B}\right]$$

$$B^* = B + \frac{m_s}{e_s}\nabla\times\left[U\hat{b} + \frac{\left\langle E\left(x^{(1)}\right)\right\rangle\times\hat{b}}{B}\right]$$

In the above expression, $B^*_{\|} = B^* \cdot \hat{b}$, and $B = B\hat{b}$, J is the adiabatic invariant.

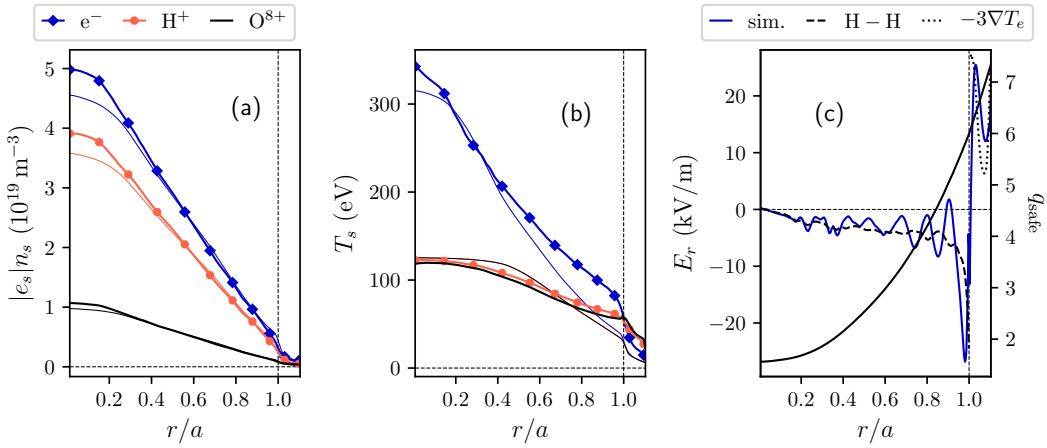

Figure 2: *a) and b) respectively show radial profiles of the charge densities and temperatures (thin: initial, bold/symbols: simulation result). c) shows the radial profiles of the radial electric field (left axis, blue: simulation result, dashed and dotted lines: analytical estimates) and safety factor profile (right axis, fixed during the simulation). All simulation results are averaged between* 100 µs *and* 140 µs. *The LCFS is shown as a vertical dashed line.*

The magnetic axis is included in the simulation domain. At the outer boundary, the logical boundary condition is used [11, 12]. The boundary is comprised of a wall at $r = a_w$, and two poloidal limiter rings at opposite toroidal positions, extending radially to the plasma radius $r = a$. The implementation presented in [12] has been modified to address stability issues as follows: the potential is set to a Dirichlet condition $\phi_{\text{bound}} = 0$ instead of a Neumann condition, and the limiters are punctual in the toroidal direction, instead of extending between two successive poloidal sections. The configuration is illustrated in Fig.1.

The experimental setting for the simulation is the tokamak FT-2 (Ioffe Institute). Experimental data interpreted with the *ASTRA* code is used as a starting point for the simulation (see the density and temperature profiles, thin lines on Fig.2a-b). The geometric parameters are as follows: $R_0 = 0.55\,\text{m}$, $a = 7.8\,\text{cm}$, $a_w = 8.7\,\text{cm}$, are the major radius, plasma radius and minor radius at the wall, respectively. The magnetic field on axis, plasma current, and loop voltage are: $B_t = 2.3\,\text{T}$, $I_p = 22.4\,\text{kA}$, $U_{\text{loop}} = 3.865\,\text{V}$. The main impurity is identified as O^{8+}, with $Z_{\text{eff}} = 2.5$. The safety factor profile is shown on Fig2c.

A snapshot simulation of turbulence is performed with these parameters for 140 µs. The profiles presented are averaged over the last 40 µs, well after the turbulence has reached its nonlinear saturation. Some relaxation of the profiles is observed (see Fig2a-b). In particular, the density and electron temperature are peaking in the core, and the temperatures are raising from

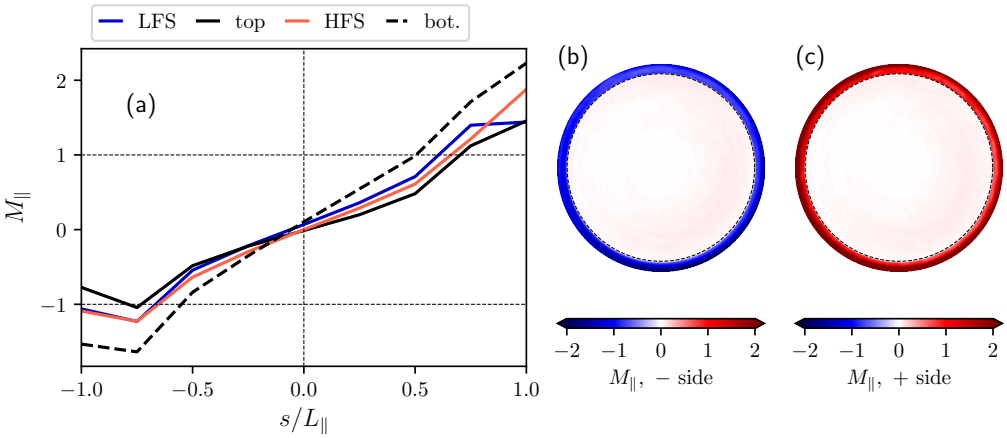

Figure 3: *a) shows parallel profiles of the parallel Mach number in the SOL, averaged over four different sectors: top, bottom, HFS, and LFS. b) and c) are poloidal sections of $M_\parallel$ at the position of a limiter, on either side. The LCFS is shown as a dashed circle.*

mid-radius to the wall. This points to inadequate heat sinks in the SOL, where the heat transported by turbulence accumulates. Conversely, the density profile in the SOL appears clamped close to its initial value, with the limiter acting as a strong particle sink.

The radial electric field obtained in the simulation is shown to match very well the radial force-balance in the confined region (Hinton-Hazeltine analytical estimate [13], dashed black line in Fig.2c), and reverses its sign is the SOL to match the sheath-governed $-3\nabla Te$ (dotted black line in Fig.2c) [3]. The values obtained on either side of the shear layer are of the order of those observed in experiments. In addition, turbulence-driven zonal flows cause oscillations around the neoclassical value in the confined region.

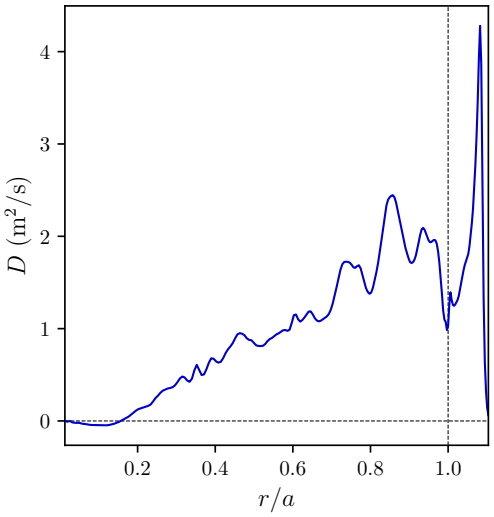

Figure 4: *Radial profile of the diffusivity from the simulation, averaged between* 100 µs *and* 140 µs. *The LCFS is shown as a vertical dashed line.*

In agreement with theoretical predictions [14], the parallel ion flow is observed to accelerate to supersonic velocities in the direction of the plates. In the context of the logical boundary condition, the sheath entrance where the supersonic condition holds true is also the boundary of the system [11]. However, we can see in Fig.3 that the ion flow can exceed the sound speed by more than a factor 2, in particular in the outermost region of the SOL. Poloidal asymmetry of the SOL flow is also observed, with Mach numbers highest in the bottom sector and lowest in the

top sector.

The very sharp shear layer shown in Fig.2c is also responsible for a weak transport barrier at the last-closed flux surface (LCFS), illustrated by the diffusivity coefficient in Fig.4, defined as $D = -\Gamma_e/\partial_r p_e$ where Γ is the particle flux. As shown on the figure, the diffusivity grows steadily towards the edge, and then collapses by a half at the LCFS.

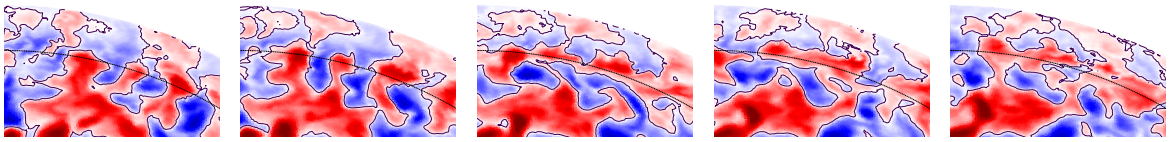

Figure 5: *Zoom on the top-LFS sector of a poloidal section of the density perturbation* $\tilde{n}_e = n_e - \bar{n}_e$*, with* $\bar{n}_e$ *the average on flux-surfaces. Time increases from left to right, by steps of* $0.45\,\mu s$*. The LCFS is shown as a dashed line.*

Perturbations are observed to cross the LCFS, where they are sheared-off by the very strong $E \times B$ flows (right to left in the confined edge, left to right in the SOL, in Fig.5). Because of the very short connection length between the two poloidal limiters (here $L_{\|} \approx 1.5\,\mathrm{m}$), the blobs originate in the confined edge and visibly decay once inside the SOL.

In conclusion, the *ELMFIRE* code has demonstrated the capacity to simulate SOL plasma and recover expected analytical results. On the other hand, shortcomings in reproducing faithfully the experimental equilibrium have been identified, calling in particular for refinements of the sources and sinks model in the SOL, such as recycling and charge exchange.

References

[1] E. J. Doyle *et al.*, Nucl. Fusion **47** (2007) S18

[2] A. Loarte *et al.*, Nucl. Fusion **47** (2007) S203

[3] P. C. Stangeby, The Plasma Boundary of Magnetic Fusion Devices, IOP Publishing, 2000

[4] F. Wagner, Plasma Phys. Control. Fusion **49** (2007) B1

[5] F. Ryter *et al.*, Nucl. Fusion **54** (2014) 083003

[6] J. A. Heikkinen *et al.*, J. Comput. Phys. **227** (2008) 5582–5609

[7] T. Korpilo, PhD Thesis, Aalto University publication series (2017)

[8] P. Niskala, PhD Thesis, Aalto University publication series (2018)

[9] P. Sosenko *et al.*, Phys. Scr. **64** (2001) 264–272

[10] L. Wang and T. S. Hahm, Phys. Plasmas **17** (2010) 082304

[11] S. Parker *et al.*, J. Comput. Phys. **104** (1993) 41–49

[12] L. Chôné *et al.*, to be published in Contrib. Plasma Phys.

[13] F. L. Hinton and R. D. Hazeltine, Rev. Mod. Phys. **48** (1976) 239

[14] P. Ghendrih *et al.*, Plasma Phys. Control. Fusion **53** (2011) 054019